Am J Cancer Res 2026;16(6):2342-2354
www.ajcr.us /ISSN:2156-6976/ajcr0172633

Original Article

Targeting ferroptosis in gefitinib-resistant HCC827 NSCLC cells using erastin

A-Young Nam[1*], Sang Hoon Joo[2*], Na Yeong Lee[1], Goo Yoon[3], Jin Woo Park[1,3], Jung-Hyun Shim[1,3,4]

[1]Department of Biomedicine, Health and Life Convergence Sciences, BK21 Four, College of Pharmacy, Mokpo National University, Muan 58554, Republic of Korea; [2]College of Pharmacy, Daegu Catholic University, Gyeongsan 38430, Republic of Korea; [3]Department of Pharmacy, College of Pharmacy, Mokpo National University, Muan 58554, Republic of Korea; [4]The China-US (Henan) Hormel Cancer Institute, Zhengzhou 450008, Henan, P. R. China. [*]Equal contributors and co-first authors.

Received March 14, 2026; Accepted May 24, 2026; Epub June 15, 2026; Published June 30, 2026

Abstract: Overcoming drug resistance remains essential for improving clinical outcomes in non-small cell lung cancer (NSCLC). This study explores the differential susceptibility of drug-resistant cancer cells, utilizing gefitinib (GEF)-resistant HCC827GR NSCLC cells as a model system. We observed that HCC827GR cells inherently display elevated levels of reactive oxygen species (ROS) and increased expression of ferroptosis-related markers when compared with GEF-sensitive cells. Accordingly, the HCC827GR lineage showed heightened responsiveness to erastin-mediated cytotoxicity, as determined by MTT and soft-agar assays. Our mechanistic investigations established that erastin treatment resulted in non-apoptotic cell death, accompanied by mitochondrial dysfunction and G2/M phase arrest in the cell cycle. In-depth analysis demonstrated that erastin notably raised intracellular iron and ROS concentrations and induced lipid peroxidation. Pretreatment with N-acetyl cysteine (NAC) validated the crucial involvement of ROS, and the use of ferrostatin-1 conclusively verified ferroptosis as the predominant mode of cell death. In summary, GEF-resistant HCC827GR cells exhibit increased sensitivity to erastin-induced ferroptosis compared with the parental line. This distinct vulnerability should be further studied as a potential therapeutic approach for targeting drug-resistant NSCLC.

Keywords: Erastin, gefitinib, drug-resistance, non-small cell lung cancer, reactive oxygen species, ferroptosis

Introduction

Lung cancer remains among the most prevalent cancers globally, accounting for nearly two million deaths annually [1]. Non-small cell lung cancer (NSCLC) constitutes the most frequently diagnosed subtype, with a 5-year survival rate of less than 30% [2]. Since the early 2000s, therapies that target receptor tyrosine kinases (RTKs), such as the epidermal growth factor receptor (EGFR), have become a central approach for the management of NSCLC [3]. Gefitinib (GEF), a first-generation EGFR tyrosine kinase inhibitor (TKI), exhibits its anticancer effects primarily by inhibiting the EGFR signaling pathway [4]. Nevertheless, the development of resistance significantly limits GEF's effectiveness in treating lung cancer patients [5]. The most extensively characterized resistance mechanism is the EGFR T790M mutation, which reduces the potency of TKIs by increasing the receptor's affinity for ATP [6]. Alongside the EGFR T790M mutation, *MET* amplification is frequently identified as a resistance mechanism. MET kinase activation facilitates continued cancer cell survival despite EGFR pathway inhibition [7]. Approaches to counteract resistance to first-generation EGFR inhibitors have included the introduction of irreversible inhibitors [8], and TKIs with specificity for mutated EGFR T790M [9]. Although several strategies have been developed to overcome resistance, considerable challenges persist, underscoring the need for ongoing research to improve NSCLC patient outcomes and survival.

The survival and death of cancer cells are influenced by multiple factors, among which reactive oxygen species (ROS) play a crucial role [10]. Cancer cells commonly exhibit increased

https://doi.org/10.62347/QRAD4785

ROS levels to take advantage of their pro-tumorigenic properties [11]. Although moderate ROS concentrations support the proliferation of cancer cells, excessive ROS accumulation may be cytotoxic and induce apoptosis [12]. To survive under oxidative stress, cancer cells initiate antioxidant defenses to shield themselves from ROS-induced cellular damage [13]. Since rapidly proliferating cancer cells maintain high ROS levels, interventions that elevate ROS production may selectively target malignant cells. Elevated ROS may induce mitochondrial membrane permeabilization [14], and the resulting mitochondrial membrane potential (MMP) loss may trigger apoptosis [15] or alternative forms of cell death [16].

Erastin acts as an inhibitor of system Xc^-. This system plays an essential role in cellular GSH supply, and its inhibition results in increased lipid peroxidation. This accumulation of lipid peroxides can subsequently initiate ferroptosis, which is a form of programmed cell death characterized by iron dependency [17]. Erastin has been demonstrated to promote ferroptosis in multiple cancer cell types [18, 19]. In this work, we evaluated the anticancer properties of erastin in HCC827 NSCLC cells, both with and without GEF-resistance. Our findings show that the GEF-resistant HCC827 cells exhibited increased sensitivity to erastin-induced ferroptosis compared to the parental cell line.

Materials and methods

Chemicals, reagents, and antibodies

Gefitinib (GEF; Cayman Chemical, MI, USA) and erastin (GlpBio Technology Inc., CA, USA) were dissolved in dimethyl sulfoxide (DMSO; Thermo Fisher Scientific, MA, USA). N-Acetyl-L-cysteine (NAC) was purchased from Sigma-Aldrich (St. Louis, MO, USA), and ferrostatin-1 (Fer-1) was obtained from Selleck Chemicals (Houston, TX, USA). Fetal bovine serum (FBS), 0.05% trypsin-EDTA (0.53 mM), and 10,000 U/mL penicillin-streptomycin (P/S) were purchased from Gibco (Carlsbad, CA, USA). Roswell Park Memorial Institute (RPMI) and Dulbecco's Modified Eagle Medium (DMEM) were obtained from Welgene (Gyeongsan-si, Gyeongsangbuk-do, Republic of Korea). HRP-conjugated anti-rabbit IgG and anti-mouse IgG secondary antibodies were purchased from Thermo Fisher Scientific (Waltham, MA, USA). Primary antibodies to β-actin (Cat # sc-47778, RRID: AB_626632), p27 (Cat # sc-56338, RRID: AB_785027), cyclin B1 (Cat # sc-7393, RRID: AB_627336), cdc2 p34 (Cat # sc-8395, RRID: AB_627225), ACSL4 (Cat # sc-365230, RRID: AB_10843105) were purchased from Santa Cruz Biotechnology (Dallas, TX, USA), while xCT/SLC7A11 (Cat # 12691, RRID: AB_2687474) and GPX4 (Cat # 59735, RRID: AB_2940796) were obtained from Cell Signaling Technology (Danvers, MA, USA).

Cell culture and treatment

The human epidermal keratinocyte cell line HEKa and the NSCLC cell line HCC827 (RRID: CVCL_2063; EGFR E746-A750 deletion) and NCI-H1975 (RRID: CVCL_1511; EGFR L858R and T790M mutation) were obtained from the American Type Culture Collection (Manassas, VA, USA). The gefitinib-resistant HCC827GR, characterized by MET amplification, was kindly provided by professor Pasi A. Jänne [20]. HEKa cells were maintained in DMEM, whereas HCC827, HCC827GR, and NCI-H1975 cells were cultured in RPMI-1640 medium. All media were supplemented with 10% FBS and 1% P/S. Cells were incubated at 37°C in a humidified incubator with 5% CO_2. HCC827GR cells were maintained in RPMI-1640 medium containing 0.1 μM gefitinib. In the experiments, cells were treated with either erastin or GEF for 24 or 48 h. When necessary, cells were pretreated with NAC (4 mM) for 3 h, or Fer-1 for 12 h prior to erastin treatment.

Cell viability assay

Following overnight attachment in 96-well plates, the cells were treated with erastin or GEF for 24 or 48 h, and the cell viability was determined using the MTT assay. Following treatment, MTT solution (Thermo Fisher Scientific, 1 mg/mL) was added to each well, and the plate was incubated at 37°C on a shaker. The resulting formazan were dissolved in dimethyl sulfoxide (DMSO), and A VARIOSKAN LUX microplate reader (Thermo Fisher Scientific) was used to measure absorbance at 570 nm.

Anchorage-independent growth assay

Soft-agar colony formation assay was conducted to evaluate effects on anchorage-independent cell growth, as previously described [21]. After 14 days of incubation, colony formation

was visualized under a light microscope (Leica, Wetzlar, Germany), and images were processed using I-Solution software (Vancouver, BC, Canada). Colonies measuring 40 μm or larger in diameter were counted and included in subsequent size distribution analyses.

Protein expression analysis

The cells were lysed using Protein Extraction Solution (iNtRON Biotechnology, Seongnam, Korea) containing protease inhibitors. Protein levels were quantified using the BCA assay (Bio-Rad, Hurcules, CA, USA). Equal amounts (10-20 μg) were resolved by SDS-PAGE and transferred to PVDF membranes (Millipore, Burlington, MA, USA). After blocking with 5% skim milk in phosphate buffered saline with 1% tween (PBST), membranes were probed with primary antibodies at 4°C overnight, and subsequently with HRP-conjugated secondary antibodies for 2 h. Detection was performed using ECL reagents and visualized on an iBright™ CL1500 system (Thermo Fisher Scientific).

Determination of intracellular ROS levels

To assess intracellular ROS accumulation, cells were exposed with 5 μM CellROX™ Green Reagent (Invitrogen, Carlsbad, CA, USA) at 37°C for 30 minutes under light-protected conditions. After incubation, excess dye was removed by washing with phosphate buffered saline (PBS), and fluorescence was measured using a MACSQuant 16 Analyzer (Miltenyi Biotec, Bergisch Gladbach, Germany).

Cell cycle analysis

To analyze cell cycle distribution, cells were stained with propidium iodide (PI) and subjected to flow cytometry. Briefly, cells were fixed in 70% ethanol at -20°C overnight, and then washed with PBS, incubated with RNase A (50 μg/mL) for 15 minutes at room temperature. PI solution was added to the cell suspension prior to analysis. DNA content was then quantified by flow cytometry using a MACSQuant 16 Analyzer (Miltenyi Biotec).

Quantification of Fe^{2+} levels

Intracellular Fe^{2+} levels were measured using the FerroOrange probe (1 μM; Dojindo Laboratories, Kumamoto, Japan) according to the manufacturer's instructions with minor modifications. Cells were stained in Hank's balanced salt solution at 37°C for 15-30 minutes in the dark. After washing, fluorescence was acquired using a MACSQuant Analyzer 16 (Miltenyi Biotec) at 543/580 nm.

Detection of lipid ROS

Lipid peroxidation was assessed using the fluorescent probe BODIPY™ 581/591 C11 (Thermo Fisher Scientific). After treatment, cells were incubated with 2.5 μM BODIPY™ C11 dye diluted in RPMI medium for 15 minutes at 37°C in the dark. The stained cells were harvested and washed twice in PBS. Fluorescence changes indicative of lipid peroxidation were detected using a MACSQuant 16 Analyzer.

Intracellular glutathione assay

Intracellular glutathione (GSH) levels were measured using the GSH/GSSG-Glo™ Assay kit (Promega, WI, USA) according to the manufacturer's instructions. Cells plated in 96-well plates were treated with erastin (1, 2, and 3 μM) for 48 h, and lysed using the provided lysis reagent. Luciferin Generation Reagent (50 μL) was added to each well and incubated for 30 min at room temperature, followed by the addition of 100 μL Luciferin Detection Reagent and incubation for 15 min. Luminescence was measured using a Centro LB 960 plate reader (Berthold Technologies, Bad Wildbad, Germany). GSH levels were calculated from a glutathione standard curve, normalized to protein concentration determined by BCA assay, and expressed relative to the untreated control group.

Glutathione peroxidase activity assay

Glutathione peroxidase (GPx) activity was measured using a Glutathione Peroxidase Assay Kit (Abcam, Cambridgeshire, UK) according to the manufacturer's instructions. Briefly, erastin-treated cells were washed with cold PBS, and lysed in the assay buffer. The lysates were centrifuged at 13,000 rpm for 15 min at 4°C, and the supernatants were collected for analysis. Briefly, 20 μL of each sample was mixed with reaction mixture (containing NADPH, glutathione reductase, and glutathione) following incubation at room temperature for 15 min. Then cumene hydroperoxide was added, fol-

lowed by absorbance measurement at 340 nm using a VARIOSCAN LUX microplate reader (Thermo Fisher). GPx activity was calculated based on the consumption of NADPH according to the manufacturer's protocol. GPx activity was normalized by protein concentration obtained from BCA assay.

Mitochondrial membrane potential (MMP) analysis

MMP was assessed using JC-1 dye (10 μg/mL) following Erastin treatment. NSCLC cells were stained at 37°C for 30 minutes in the dark, washed with PBS, and analyzed by flow cytometry (MACSQuant VYB, Miltenyi Biotec). Data processing was performed using MACSQuantify software.

Analysis of apoptotic cell death

Apoptosis was assessed by Annexin V-FITC/PI staining. After treatment, cells were resuspended in binding buffer, stained according to the manufacturer's instructions, and incubated for 15 minutes in the dark. Fluorescence was measured using MACSQuant Analyzer 16 (Miltenyi Biotec) and analyzed with MACSQuantify software.

Data analysis

The statistical study was performed using KaleidaGraph version 4.5 (Synergy Software, Reading, PA, USA). Data were reported as the mean ± standard deviation (SD). One-way ANOVA followed by Tukey's post-hoc test, and two-way ANOVA followed by Šídák's multiple comparisons test, were performed to evaluate the significance of differences. Statistical significance between two groups was analyzed using an unpaired Student's t-test with Welch's correction. *P*-value less than 0.05 was employed as the statistical significance criterion. IC_{50} values were calculated by nonlinear regression analysis using GraphPad Prism 10.3 (GraphPad Software, CA, USA) based on three independent experiments.

Results

The GEF-resistant NSCLC cell lineage shows increased expression of ferroptosis-related markers and ROS

To compare protein expression involved in ferroptosis between HCC827 and HCC827GR cells, western blotting was performed (**Figure 1A**). SLC7A11, GPX4, and ACSL4 expression levels were elevated by 2.4-, 3.2-, and 1.9-fold, respectively, in HCC827GR cells compared to HCC827 cells (**Figure 1B-D**). CellROX Green-based flow cytometry was used to measure basal intracellular ROS in both cell lines (**Figure 1E**). The basal ROS level in HCC827GR cells was roughly 4.3-fold higher than in HCC827 cells (HCC827: 14.5%, HCC827GR: 63.5%). Lipid peroxidation was evaluated by flow cytometry using BODIPY-C11. The level of lipid ROS in HCC827GR cells was approximately 3.7-fold greater than that in HCC827 cells (HCC827: 12.3%, HCC827GR: 45.7%).

The GEF-resistant NSCLC cell lineage demonstrates enhanced sensitivity to erastin-induced cytotoxicity

First, we assessed the proliferation of NSCLC cells using the MTT assay. Treatment with erastin for 24 and 48 hours suppressed the growth of both HCC827 and HCC827GR cells relative to the vehicle control (**Figure 2A**). The IC_{50} values of erastin at 48 hours were 7.6 μM for HCC827 cells, 2.1 μM for HCC827GR cells, and 3.4 μM for NCI-H1975, respectively. Exposure to GEF (1 μM) reduced HCC827 cell proliferation to 49.9% at 24 hours and 20.6% at 48 hours (**Figure 2B**). In contrast, HCC827GR cells maintained proliferation rates of 99.2% and 97.9% under the same conditions, confirming the resistance of this cell line to GEF. Similarly, NCI-H1975 cells also maintained a high proliferation rate of 94.0% and 92.7% under the same conditions (Supplementary Figure 1). To investigate the cytotoxicity of erastin in HEKa cells, viability was evaluated following treatment with increasing concentrations of erastin (0-12 μM) for 24 and 48 hours using the MTT assay. The findings indicated that erastin did not decrease the viability of HEKa cells (**Figure 2C**). The impact of erastin on anchorage-independent growth was determined by a soft agar assay (**Figure 2D**). In HCC827 cells, erastin treatment at 1, 2, 3, and 9 μM reduced colony numbers to 93.7%, 93.7%, 88.6%, and 0.0%, respectively, when compared to the vehicle control. Corresponding colony sizes decreased to 88.3%, 80.8%, 78.2%, and 0.0%, respectively. In HCC827GR cells, colony numbers were reduced to 8.5%, 0.0%, 0.0%, and 0.0% at 1, 2, 3, and 9 μM erastin, respectively, and colony size similarly decreased to 77.8%, 0.0%, 0.0%, and 0.0%. Upon GEF treatment (1 μM), the

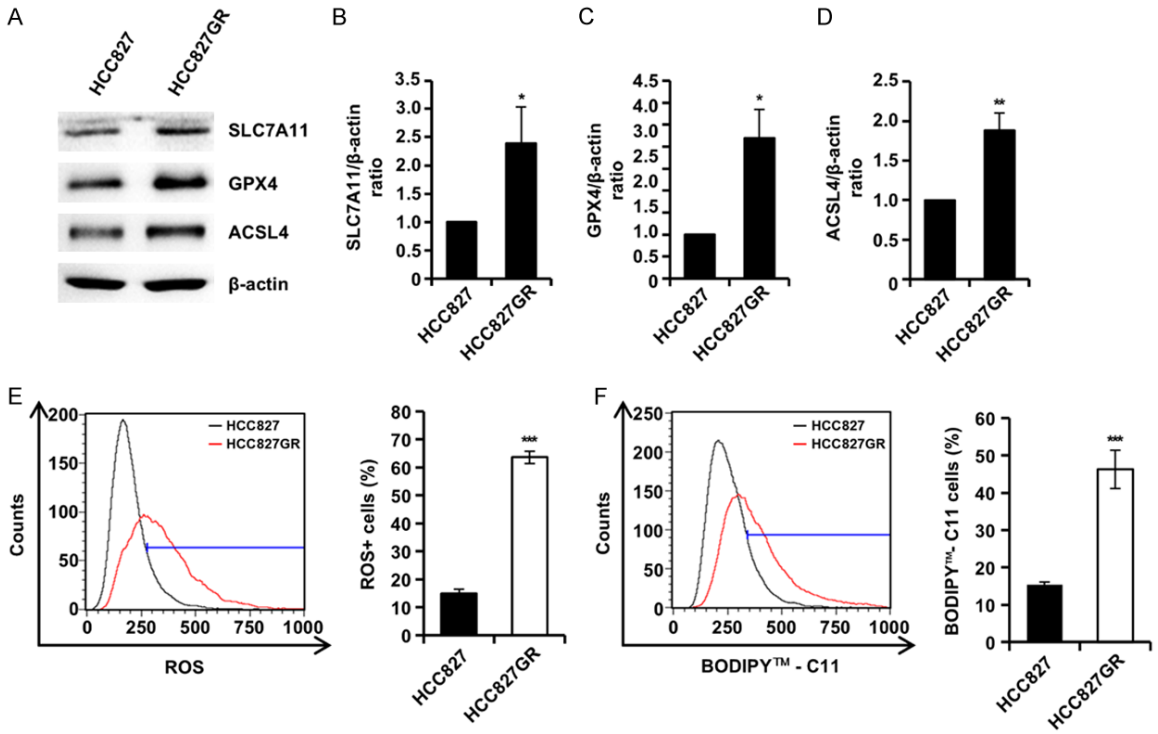

Figure 1. Ferroptosis-related protein expression and oxidative stress. (A-D) Western blot analysis of protein expression levels in HCC827 and HCC827GR cells. (A) Representative western blot image. The relative expression levels of SLC7A11 (B), GPX4 (C), and ACSL4 (D) were normalized to the β-actin level. Data are shown as the mean ± standard deviation (n=3). *P<0.05 and **P<0.01 compared with HCC827 cells (*P* values calculated using unpaired Student's t-test). (E) Basal intracellular ROS levels in HCC827 and HCC827GR cells, assessed by flow cytometry using CellROX Green. Left: representative flow cytometry histogram. Right: relative ratios of ROS+ cells. (F) Basal lipid peroxidation was measured in HCC827 and HCC827GR cells by flow cytometry using BODIPY-C11 staining. Left: representative histogram. Right: relative ratios of BODIPY-C11+ cells. Data are shown as the mean ± standard deviation (n=3). ***P<0.001 compared with HCC827 cells (*P* values calculated using unpaired Student's t-test).

number and size of HCC827 colonies both fell to 0.0%, whereas those for HCC827GR cells remained at 93.1% and 97.4%, respectively (**Figure 2E** and **2F**).

Erastin induces G2/M phase cell cycle arrest in NSCLC cells

To investigate the impact of erastin on cell cycle progression, flow cytometry analysis with PI staining was conducted on NSCLC cells exposed to erastin (1, 2, and 3 μM) or gefitinib (1 μM) for 48 h (**Figure 3A**). In HCC827GR cells, the percentage of cells in the G0/G1 phase decreased from 70.0% in the controls to 66.7%, 61.9%, and 55.0% after treatment with 1, 2, and 3 μM erastin, respectively. Conversely, HCC827 cells exhibited percentages of 72.4% (control), 72.6%, 73.3%, and 73.4% after erastin treatment at 1, 2, and 3 μM, reflecting no substantial alteration. For HCC827GR cells, the proportion of cells in the G2/M phase increased from 22.5% (control) to 25.0%, 28.0%, and 32.3% following erastin administration at increasing concentrations. In contrast, the corresponding values for HCC827 cells were 16.2% (control), 16.3%, 15.7%, and 15.3% for the same erastin exposures, again indicating minimal change (**Figure 3B** and **3C**). Following treatment with 1 μM gefitinib, HCC827 cells exhibited an increase in G0/G1 phase cell percentage from 72.4% (control) to 87.1%, accompanied by reductions in S and G2/M phases from 11.4% and 16.2% to 4.1% and 8.8%, respectively. By contrast, in HCC827GR cells, the proportions in G0/G1, S, and G2/M phases were 70.0%, 7.5%, and 22.5% (control), and 71.4%, 7.5%, and 21.1% after gefitinib treatment, revealing negligible variation. Western blotting to assess p27, cyclin B1, and cdc2 protein levels showed stable expression in HCC827 cells, while in HCC827GR cells, p27 expression increased

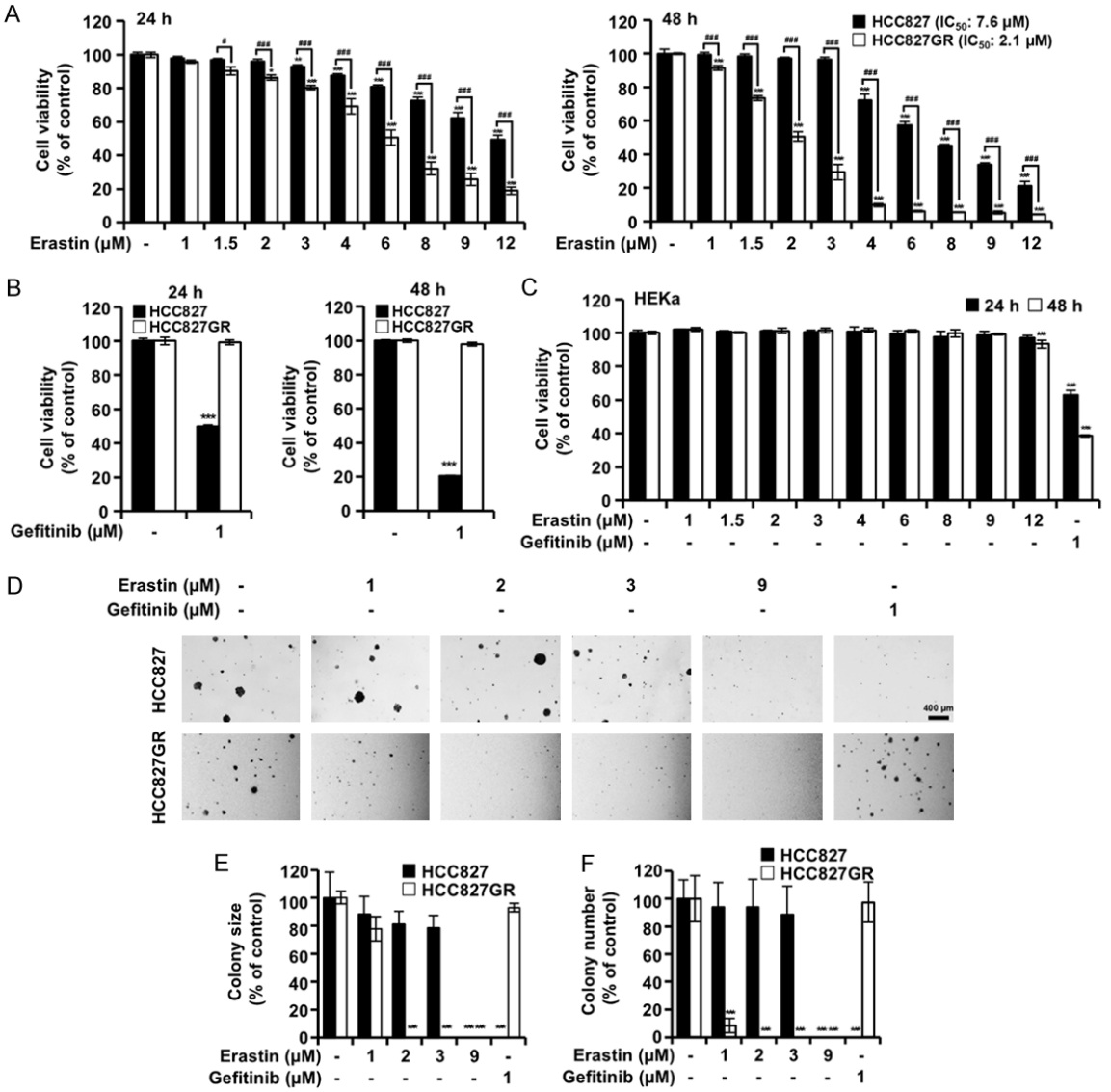

Figure 2. MTT cell viability assay and soft-agar colony formation assay. A-C. HCC827, HCC827GR, and HEKa cells were exposed to the indicated concentrations of erastin or gefitinib (GEF) for either 24 h or 48 h. Cell viability was assessed via the MTT assay, and IC_{50} values were determined. A. Cell viability of HCC827 (closed bar) and HCC827GR (open bar) cells treated with erastin for 24 h (left) and 48 h (right). B. Cell viability of HCC827 and HCC827GR cells treated with GEF for 24 h and 48 h. C. Cell viability of HEKa cells exposed to erastin for 24 h (closed bar) and 48 h (open bar). D, E. HCC827 and HCC827GR cells, following treatment with erastin or GEF at indicated concentrations, were cultured on soft-agar plates for 14 days, after which both colony number and size were analyzed using I-Solution software. D. Representative microscopy images. E. Bar graph representing the relative size of colonies. F. Bar graph representing the relative colony number. Results are shown as mean ± standard deviation (n=3). **P<0.01, and ***P<0.001 compared with the vehicle control (*p* values based on Tukey's post hoc test). #P<0.05 and ###P<0.001 between the erastin-treated HCC827 and HCC827GR groups (two-way ANOVA followed by Šídák's multiple comparisons test).

and cyclin B1 and cdc2 levels were reduced following erastin exposure (**Figure 3D**).

Erastin induces non-apoptotic mitochondrial dysfunction in NSCLC cells

To determine whether erastin triggers mitochondrial dysfunction and apoptosis in NSCLC cells, flow cytometric analysis using JC-1 staining was performed and mitochondrial membrane potential (MMP) measured in NSCLC cells treated with erastin (**Figure 4A**). In HCC827 cells, the fraction of cells with depolarized mitochondrial membranes increased marginally from 5.5% (control) to 6.7%, 7.3%, and 8.3% after erastin at 1, 2, and 3 μM. However, in

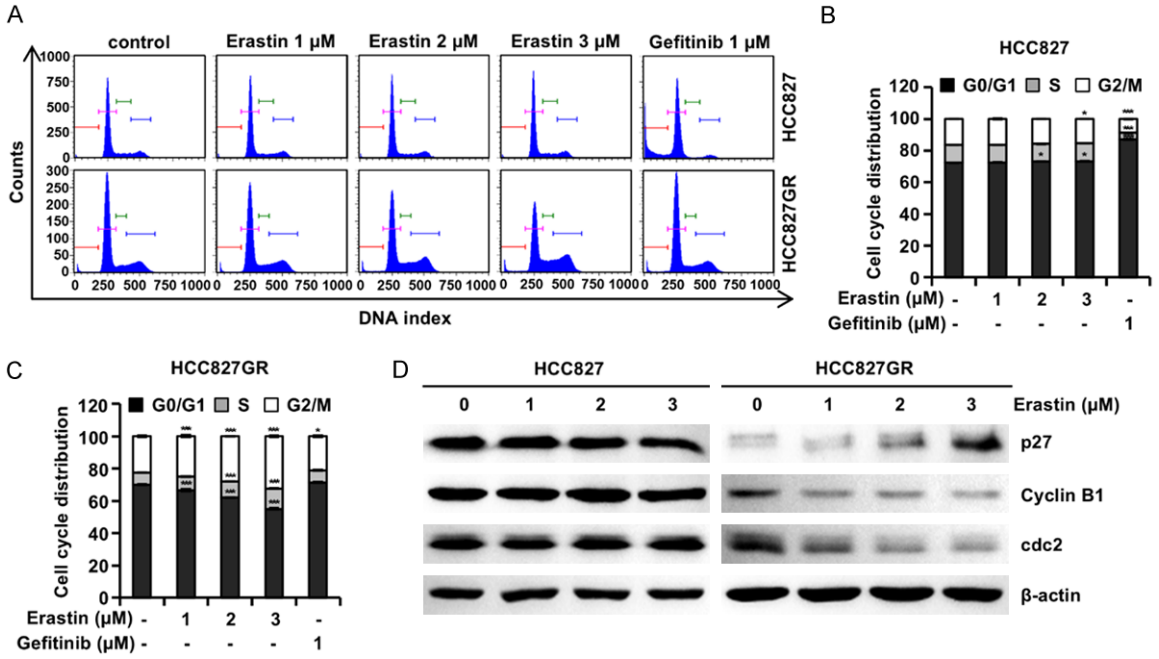

Figure 3. Cell cycle analysis. HCC827 and HCC827GR cells were exposed to the indicated concentrations of erastin or GEF for 48 h and subsequently analyzed by flow cytometry with PI staining or by western blotting. (A) Representative histogram from flow cytometry. (B, C) Bar graphs display the distribution of HCC827 (B) and HCC827GR (C) cells at G0/G1, S, and G2/M phases after treatment. Results are shown as mean ± standard deviation (n=3). *P<0.05 and ***P<0.001 compared to the control group (*p* values were obtained via Tukey's post hoc test). (D) Expression levels of p27, cyclin B1, and cdc2 proteins were assessed by immunoblotting.

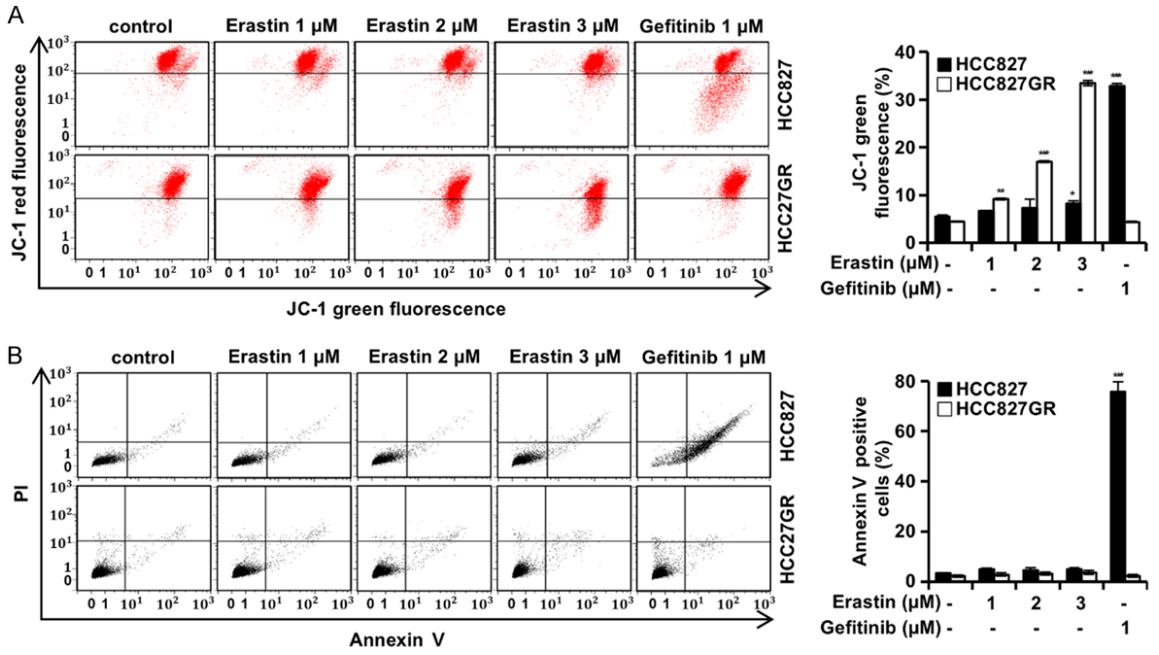

Figure 4. Mitochondrial membrane potential (MMP) and annexin V. HCC827 and HCC827GR cells were exposed to the indicated concentrations of erastin or GEF for 48 h and analyzed by flow cytometry using JC-1 staining and annexin V-FITC/propidium iodide double-staining. A. Left: Representative flow cytometry dot plots following JC-1 staining. Right: Relative ratio of JC-1 green cells. B. Left: Representative flow cytometry dot plots following annexin V-FITC/propidium iodide double-staining. Right: Relative ratio of annexin V + cells. Results are presented as mean ± standard deviation (n=3). *P<0.05, **P<0.01, and ***P<0.001 versus control (*p* values based on Tukey's post hoc test).

HCC827GR cells, this fraction rose markedly from 4.4% (control) to 9.2%, 17.0%, and 35% for the same erastin doses. To assess whether MMP disruption resulted in apoptosis, flow cytometry using Annexin V-FITC/PI double-staining was carried out (**Figure 4B**). Erastin treatment caused no significant change in the apoptotic cell fraction. By contrast, GEF treatment led to a pronounced increase in apoptotic cells in HCC827 cells, from 3.4% to 75.8%, yet no similar effect was seen in HCC827GR cells.

Erastin triggers ferroptotic cell death in NSCLC cells

To investigate whether erastin increases cellular iron levels, flow cytometry analysis utilizing FerroOrange was conducted (**Figure 5A**). In HCC827 cells, the intracellular iron levels remained relatively consistent, ranging from the control value of 14.7% to 12.4%, 15.9%, and 18.9% following erastin treatments at 1, 2, and 3 μM, respectively. Conversely, in HCC827GR cells, iron levels increased markedly from the control level of 17.5% to 42.3%, 56.9%, and 73.7% after exposure to erastin at 1, 2, and 3 μM, respectively. GEF treatment (1 μM) led to elevated iron levels at 31.9% in HCC827 cells and 27.5% in HCC827GR cells. Subsequently, to assess the impact of erastin treatment on lipid peroxidation, NSCLC cells were subjected to flow cytometry using BODIPY-C11 following exposure to erastin (1, 2, and 3 μM) or gefitinib (1 μM) for 48 h (**Figure 5B**). In HCC827 cells, the level of lipid peroxidation showed minimal change, rising modestly from 12.7% in the control to 15.8%, 19.9%, and 25.0% after erastin treatment at 1, 2, and 3 μM, respectively. Conversely, the lipid peroxidation level in HCC827GR cells increased markedly from 18.5% (control) to 35.7%, 47.9%, and 75.0% after treatment with erastin at 1, 2, and 3 μM, respectively. In addition, lipid peroxidation level in NCI-H1975 cells increased from 18.6% in untreated controls to 20.4%, 35.5%, 43.5%, and 69.3% following treatment with 1, 2, 3, and 4 μM erastin, respectively (Supplementary Figure 1). In contrast, GEF treatment (1 μM) resulted in lipid peroxidation levels of 30.2% and 17.7% in HCC827 and HCC827GR cells, respectively. Western blot analysis indicated that protein expression levels associated with ferroptosis were unchanged in HCC827 cells; however, SLC7A11 and GPX4 expression decreased while ACSL4 expression increased in HCC827GR cells (**Figure 5C**). To further investigate erastin-induced ferroptosis, cell viability in NSCLC cells treated with erastin was measured using an MTT assay, with or without a 12 h preincubation with Fer-1 (**Figure 5D**). Treatment with 9 μM erastin reduced HCC827 cell viability to 28.7% of control levels, whereas 3 μM erastin reduced HCC827GR cell viability to 25.3%. Pretreatment with Fer-1 (5 μM for HCC827 and 4 μM for HCC827GR cells) restored cell viability to 73.7% and 86.0%, respectively. Because erastin inhibits the cystine/glutamate antiporter system Xc^- [17], intracellular GSH levels were subsequently evaluated in HCC827 and HCC827GR cells. As shown in **Figure 5E**, treatment with erastin at 1, 2, and 3 μM decreases the GSH level in HCC827 cells to 0.68, 0.45, 0.4, respectively, compared with untreated control. In HCC827GR cells, treatment with 1, 2, and 3 μM erastin markedly reduced GSH levels to 0.19, 0.1, and 0.01 of untreated control, respectively (**Figure 5E**). Furthermore, to determine whether erastin treatment alters GPx activity in NSCLC cells, we measured GPx activity after 48 h exposure to erastin. In HCC827 cells, GPx activity decreased to 95.2%, 42.3%, and 33.1% following treatment with 1, 2, 3 μM erastin, respectively, while HCC827GR cells showed reductions of 24.1%, 10.4%, and 8.6%, respectively, compared with the untreated control (**Figure 5F**). GPx activity in NCI-H1975 cells decreased to 37.6%, 34.4%, 24.0%, and 19.3% at 1, 2, 3, and 4 μM erastin, respectively (Supplementary Figure 1).

Erastin-induced intracellular ROS promotes ferroptosis in NSCLC cells

Flow cytometry with CellROX Green was performed to determine if increased iron levels were associated with changes in intracellular ROS levels (**Figure 6A**). In HCC827 cells, ROS levels exhibited minimal variation, rising from a control level of 12.3% to 12.5%, 12.9%, and 15.4% after erastin treatment at 1, 2, and 3 μM, respectively. In contrast, ROS levels in HCC827GR cells rose significantly, from a control level of 16.4% to 32.0%, 41.8%, and 50.0% following corresponding erastin treatments. Furthermore, erastin treatment induced ROS accumulation in NCI-H1975 cells, with ROS levels increasing from 18.0% in untreated control to 27.5%, 36.3%, 43.2%, and 64.7% following treatment with 1, 2, 3, and 4 μM erastin,

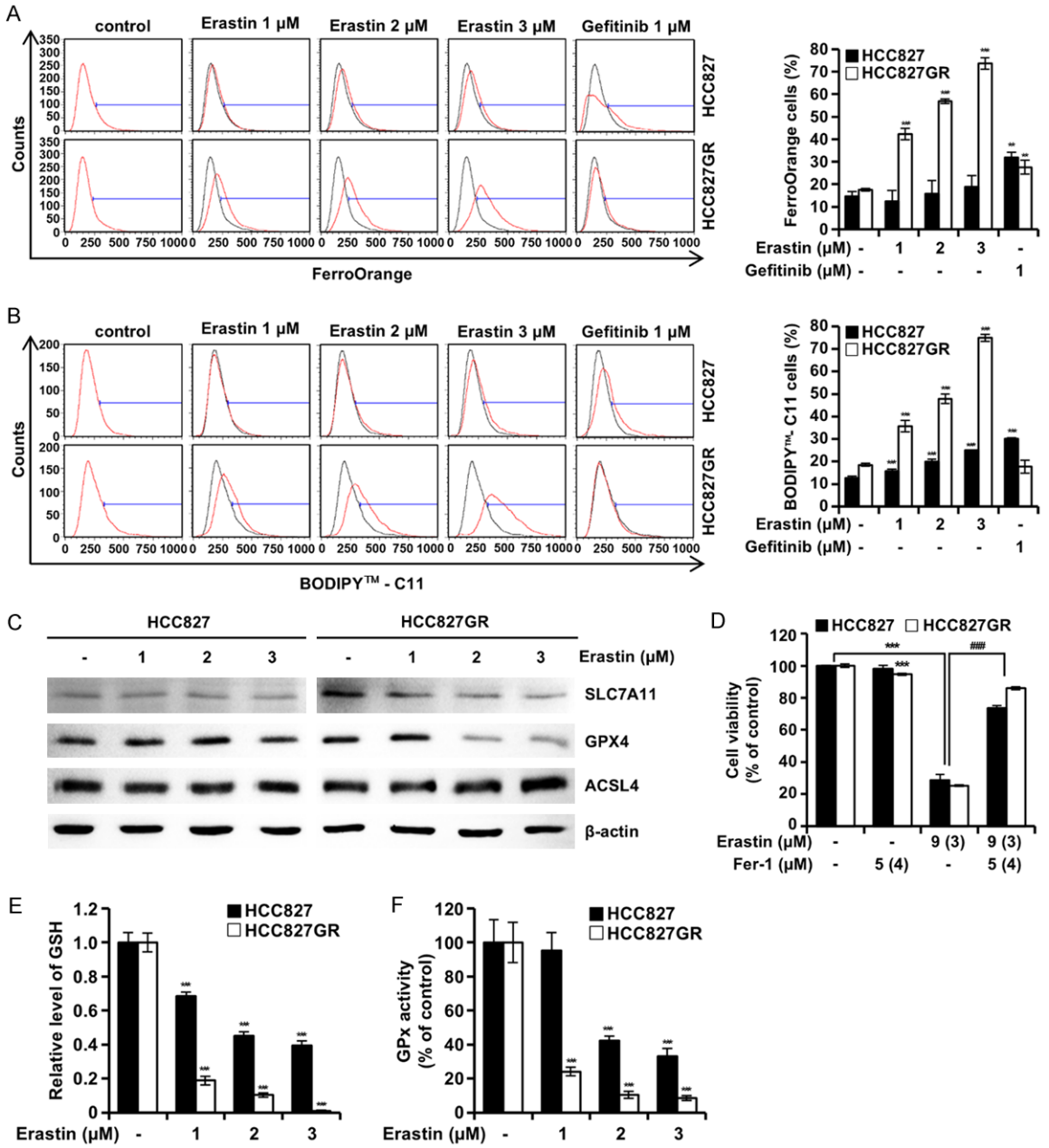

Figure 5. Intracellular iron and lipid peroxidation levels. A, B. HCC827 and HCC827GR cells were treated with the indicated concentrations of erastin or GEF for 48 h and analyzed by flow cytometry using FerroOrange and BODIPY-C11. A. Left: representative flow cytometry histogram obtained with FerroOrange. Right: quantification of the relative percentages of FerroOrange-positive cells. B. Left: representative flow cytometry histogram analyzed using BODIPY-C11. Right: quantification of the relative percentages of BODIPY-C11+ cells. C. The protein expression of SLC7A11, GPX4, and ACSL4 was assessed by immunoblotting. D. Cells were pretreated with or without Fer-1, a ferroptosis inhibitor, for 12 h, followed by erastin exposure for 48 h. Cell viability was evaluated by the MTT assay. E, F. Cells were treated with 1, 2, and 3 μM erastin for 48 h. E. Relative GSH levels. F. Relative GPx activity. Data are presented as mean ± standard deviation (n=3). **P<0.01 and ***P<0.001 vs. control group. ###P<0.001 vs. erastin-treated group (*p* values based on Tukey's post hoc test).

respectively (Supplementary Figure 1). After GEF treatment, intracellular ROS levels were 29.2% in HCC827 cells and 15.6% in HCC827GR cells, respectively. To clarify the role of ROS generation in erastin-induced cytotoxicity, cell viability was measured via MTT assay in eras-

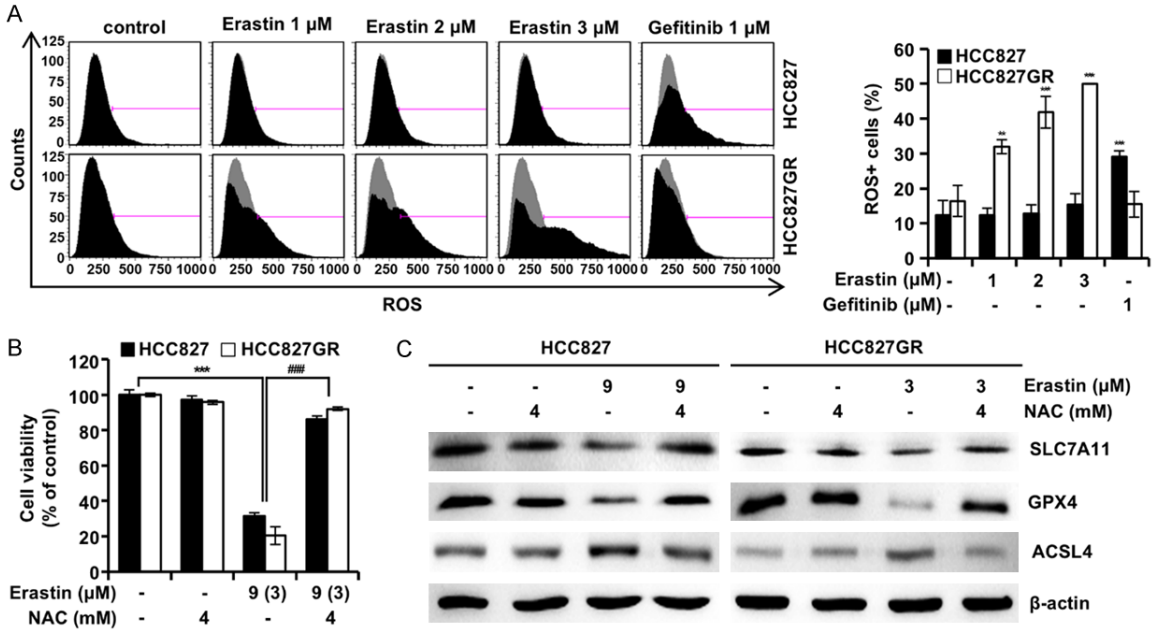

Figure 6. Intracellular ROS level. A. HCC827 and HCC827GR cells were treated with the indicated concentrations of erastin or GEF for 48 h and subjected to flow cytometry using CellRox Green or western blot analysis. Left: representative flow cytometry histogram. Right: quantification of the relative percentages of ROS-positive cells. B, C. Cells were pretreated with or without NAC for 3 h, then treated with erastin for 48 h. B. Cell viability was assessed by the MTT assay. Data are presented as mean ± standard deviation (n=3). **P<0.01 and ***P<0.001 vs. control group. ###P<0.001 vs. erastin treated group (*p* values calculated using Tukey's post hoc test). C. Western blot analysis for SLC7A11, GPX4, and ACSL4.

tin-treated NSCLC cells with or without NAC pretreatment (4 mM) for 3 h. Cell viability, which declined to 31.5% in HCC827 (erastin 9 μM) and 20.3% in HCC827GR (erastin 3 μM), was restored to 86.2% and 92.0%, respectively, following NAC pretreatment (**Figure 6B**). Western blot analysis demonstrated that NAC pretreatment reversed the reduction in SLC7A11 and GPX4 and the elevation in ACSL4 levels (**Figure 6C**).

Discussion

This study investigates the differential vulnerability of drug-resistant cancer cells as a potential approach to overcoming anticancer resistance. The GEF-resistant HCC827 NSCLC cell line shows increased expression of SLC7A11, GPX4, and ACSL4 (**Figure 1A-D**). Elevation of these proteins is hypothesized to provide protection against heightened ROS levels. Consistently, the proportion of ROS+ cells was approximately five times greater in HCC827GR cells (**Figure 1E**). Lipid peroxidation was also elevated in the GEF-resistant line (**Figure 1F**). Persistently high lipid peroxidation in HCC827GR cells results in a vulnerable metabolic condition, making even minor increases in ROS potentially lethal. Thus, this specific susceptibility may serve as an attractive target for ROS-inducing anticancer therapies. Upon recognizing this metabolic discrepancy, erastin cytotoxicity was assessed in both HCC827 and HCC827GR cells via the MTT cell viability and soft-agar assays (**Figure 2**). While erastin reduced viability in each cell type, there were notable differences in response. The IC_{50} for HCC827 cells was 11.7 μM following 24 hours of treatment, which was roughly double the IC_{50} found in HCC827GR cells (5.8 μM). Importantly, after 48 hours of treatment, the IC_{50} for HCC827GR cells declined significantly to 2.1 μM, while that for HCC827 cells was 7.6 μM, demonstrating a difference of greater than three-fold. Erastin exhibited lower IC_{50} values in the GEF-resistant NCI-H1975 cells (5.2 μM at 24 h, 3.4 μM at 48 h) than in the GEF-sensitive HCC827 cells (Supplementary Figure 1). As a result, 3 μM erastin was used to induce cell death in HCC827GR, while 9 μM was used for HCC827 cells. Although erastin was able to induce cytotoxicity in HCC827 cells at the

applied concentrations irrespective of GEF-resistance, similar doses did not affect HEKa cells, indicating that erastin's cytotoxic action is specific to cancer cells. Additionally, the GEF sensitivity of HCC827 cells and the GEF resistance of HCC827GR cells were confirmed by both the MTT cell viability and soft-agar assays.

Various anticancer drugs exert cytotoxic effects in cancer cells by modulating the cell cycle. The regulation of the cell cycle contributes to the cytotoxicity induced by anticancer drugs [22]. Cell cycle analysis demonstrated a marked reduction in the proportion of cells in the G0/G1 phase and an elevation in the G2/M phase in HCC827GR cells following erastin treatment (1, 2, 3 μM); these effects were not detected in HCC827 cells (**Figure 3**). In addition, western blot analysis revealed that erastin increases the level of the CDK inhibitor p27 [23], while simultaneously decreasing the levels of cyclin B1 and CDK1 [24]. These findings suggest that erastin disrupts cell cycle progression in HCC827GR cells by targeting the G2/M phase. In contrast, GEF treatment modified cell cycle distribution in HCC827 cells, but such alterations were absent in HCC827GR cells. Collectively, these results indicate that HCC827GR cells exhibit greater sensitivity to erastin-induced cytotoxicity than HCC827 cells, thereby confirming the resistance of HCC827GR cells to GEF.

Disruption of the mitochondrial membrane [25] can have severe implications for cell fate by eliminating functional energy-generating processes within the cell. JC-1 staining demonstrated a higher proportion of cells with disrupted or depolarized mitochondrial membranes among HCC827GR cells after erastin exposure (1, 2, and 3 μM) (**Figure 4A**). This phenomenon was not observed in HCC827 cells. In contrast, GEF treatment resulted in mitochondrial membrane depolarization in HCC827 cells, but this effect did not occur in HCC827GR cells. Notably, loss of MMP [15] was not associated with apoptosis during erastin-induced cytotoxicity. Annexin V-PI double staining indicated that neither HCC827 nor HCC827GR cells underwent apoptosis after erastin administration, in contrast to the apoptosis observed in HCC827 cells treated with GEF (**Figure 4B**). These findings indicate that erastin-mediated mitochondrial dysfunction is non-apoptotic, suggesting involvement of necroptosis or ferroptosis. An increase in cellular iron level constitutes a key feature of ferroptosis [26]. FerroOrange staining showed a pronounced elevation of intracellular iron levels following erastin (1, 2, and 3 μM) administration in HCC827GR cells, but not in HCC827 cells (**Figure 5A**). The rise in cellular iron paralleled an increase in reactive oxygen species (ROS) as detected by CellROX Green staining (**Figure 6A**). Erastin significantly increased intracellular ROS accumulation in NCI-H1975 cells (Supplementary Figure 1). Erastin-induced cytotoxicity was abrogated by pretreatment with NAC (4 mM), a reactive oxygen species scavenger (**Figure 6B**). Furthermore, western blotting revealed that NAC pretreatment restored GPX4 and SLC7A11 levels and attenuated the induction of ACSL4 (**Figure 6C**). Lipid peroxidation constitutes another hallmark of ferroptosis [26]. BODIPY-C11 staining demonstrated an elevated extent of lipid peroxidation after erastin (1, 2, and 3 μM) exposure in HCC827GR and NCI-H1975 cells, an effect not observed in HCC827 cells (**Figure 5B** and Supplementary Figure 1). Western blot analysis demonstrated that erastin treatment elevated the expression of ACSL4, a factor that promotes ferroptosis [27], in HCC827GR cells, while the expression levels of SLC7A11 and GPX4 were reduced (**Figure 5C**). Interestingly, erastin decreased GPx activity and GSH levels more prominently in gefitinib-resistant HCC827GR cells than in gefitinib-sensitive HCC827 cells in a dose-dependent manner (**Figure 5E**, **5F**). Consistently, erastin also markedly reduced GPx activity in NCI-H1975 cells (Supplementary Figure 1). In contrast to ACSL4, both SLC7A11 and GPX4 protect against ferroptosis through the provision of antioxidant GSH [28]. Paradoxically, SLC7A11 and GPX4 (key anti-ferroptotic proteins) were elevated in the more ferroptosis-sensitive HCC827GR cells. We speculate that this upregulation reflects a compensatory response to chronic oxidative stress that is insufficient to maintain redox balance under erastin challenge. Consistent with this interpretation, parental HCC827 cells were relatively resistant, showing minimal cytotoxicity at 3 μM erastin and requiring 9 μM to induce significant cell death. When the parental cell line of HCC827 and HCC827GR cells were compared, erastin 9 μM and 3 μM were used, respectively (**Figures 5D** and **6B**). While this equitoxic approach standardized initial cell death across lines, the disparity in absolute

erastin concentrations (9 μM vs. 3 μM) means that differences in the magnitude of rescue should be interpreted with caution, as they may be influenced by drug load rather than intrinsic cellular mechanics. Anyhow, this cytotoxic effect was abolished by prior administration of Fer-1, a selective ferroptosis inhibitor (**Figure 5D**), or NAC (**Figure 6B**). These results suggest that the cytotoxicity induced by erastin treatment is primarily mediated by ferroptosis.

In conclusion, we established that HCC827GR cells exhibit increased ROS production and higher levels of proteins associated with ferroptosis. HCC827GR cells display greater susceptibility to erastin-induced cytotoxicity. Treatment with erastin leads to G2/M phase cell cycle arrest, non-apoptotic mitochondrial dysfunction, enhanced iron accumulation and ROS production, lipid peroxidation, and ferroptotic cell death. Compared to the GEF-sensitive parental HCC827 cells, the GEF-resistant NSCLC HCC827GR cells are significantly more susceptible to cytotoxic effects induced by erastin. This increased sensitivity may offer a potential strategy for selectively targeting drug-resistant cancer cells and should be further investigated.

Acknowledgements

This work was supported by the National Research Foundation of Korea (NRF) grants funded by the Korea government (MSIT) (RS-2022-NR070862 and RS-2024-00336900).

Disclosure of conflict of interest

None.

Abbreviations

NSCLC, non-small cell lung cancer; ROS, reactive oxygen species; MTT, 3-(4,5-dimethylthiazol-2-yl)-2,5-diphenyltetrazolium bromide; NAC, N-acetyl-L-cysteine; MMP, mitochondrial membrane potential.

Address correspondence to: Jung-Hyun Shim and Jin Woo Park, Department of Pharmacy, College of Pharmacy, Mokpo National University, Muan 58554, Republic of Korea. Tel: +82-61-450-2684; Fax: +82-61-450-2689; E-mail: s1004jh@mokpo.ac.kr (JHS); Tel: +82-614502704; Fax: +82-61-450-2689; E-mail: jwpark@mokpo.ac.kr (JWP)

References

[1] Siegel RL, Giaquinto AN and Jemal A. Cancer statistics, 2024. CA Cancer J Clin 2024; 74: 12-49.

[2] Ganti AK, Klein AB, Cotarla I, Seal B and Chou E. Update of incidence, prevalence, survival, and initial treatment in patients with non-small cell lung cancer in the US. JAMA Oncol 2021; 7: 1824-1832.

[3] Kris MG, Natale RB, Herbst RS, Lynch TJ Jr, Prager D, Belani CP, Schiller JH, Kelly K, Spiridonidis H, Sandler A, Albain KS, Cella D, Wolf MK, Averbuch SD, Ochs JJ and Kay AC. Efficacy of gefitinib, an inhibitor of the epidermal growth factor receptor tyrosine kinase, in symptomatic patients with non-small cell lung cancer: a randomized trial. JAMA 2003; 290: 2149-2158.

[4] Kosaka T, Yamaki E, Mogi A and Kuwano H. Mechanisms of resistance to EGFR TKIs and development of a new generation of drugs in non-small-cell lung cancer. J Biomed Biotechnol 2011; 2011: 165214.

[5] Engelman JA and Janne PA. Mechanisms of acquired resistance to epidermal growth factor receptor tyrosine kinase inhibitors in non-small cell lung cancer. Clin Cancer Res 2008; 14: 2895-2899.

[6] Saldana-Rivera L, Bello M and Mendez-Luna D. Structural insight into the binding mechanism of ATP to EGFR and L858R, and T790M and L858R/T790 mutants. J Biomol Struct Dyn 2019; 37: 4671-4684.

[7] Peng LX, Jie GL, Li AN, Liu SY, Sun H, Zheng MM, Zhou JY, Zhang JT, Zhang XC, Zhou Q, Zhong WZ, Yang JJ, Tu HY, Su J, Yan HH and Wu YL. MET amplification identified by next-generation sequencing and its clinical relevance for MET inhibitors. Exp Hematol Oncol 2021; 10: 52.

[8] Hurwitz JL, Scullin P and Campbell L. Afatinib treatment in advanced non-small cell lung cancer. Lung Cancer (Auckl) 2011; 2: 47-57.

[9] Zhang H. Osimertinib making a breakthrough in lung cancer targeted therapy. Onco Targets Ther 2016; 9: 5489-5493.

[10] Schumacker PT. Reactive oxygen species in cancer: a dance with the devil. Cancer Cell 2015; 27: 156-157.

[11] Cui Q, Wang JQ, Assaraf YG, Ren L, Gupta P, Wei L, Ashby CR Jr, Yang DH and Chen ZS. Modulating ROS to overcome multidrug resistance in cancer. Drug Resist Updat 2018; 41: 1-25.

[12] Chun KS and Joo SH. Modulation of reactive oxygen species to overcome 5-fluorouracil resistance. Biomol Ther (Seoul) 2022; 30: 479-489.

[13] Marengo B, Nitti M, Furfaro AL, Colla R, Ciucis CD, Marinari UM, Pronzato MA, Traverso N and Domenicotti C. Redox homeostasis and cellular antioxidant systems: crucial players in cancer growth and therapy. Oxid Med Cell Longev 2016; 2016: 6235641.
[14] Lee SO, Joo SH, Cho SS, Yoon G, Choi YH, Park JW, Weon KY and Shim JH. Licochalcone D exerts antitumor activity in human colorectal cancer cells by inducing ROS generation and phosphorylating JNK and p38 MAPK. Biomol Ther (Seoul) 2025; 33: 344-354.
[15] Gottlieb E, Armour SM, Harris MH and Thompson CB. Mitochondrial membrane potential regulates matrix configuration and cytochrome c release during apoptosis. Cell Death Differ 2003; 10: 709-717.
[16] Kroemer G and Reed JC. Mitochondrial control of cell death. Nat Med 2000; 6: 513-519.
[17] Joo SH, Cho YY and Shim JH. Targeting ferroptosis to overcome drug resistance in cancer: molecular mechanisms and therapeutic prospects. Biomol Ther (Seoul) 2025; 34: 18-29.
[18] Wang H, Wang P and Zhu BT. Mechanism of erastin-induced ferroptosis in MDA-MB-231 human breast cancer cells: evidence for a critical role of protein disulfide isomerase. Mol Cell Biol 2022; 42: e0052221.
[19] Wei X, Huang Q, Huang J, Yu L and Chen J. Erastin induces ferroptosis in cervical cancer cells via Nrf2/HO-1 signaling pathway. Int J Immunopathol Pharmacol 2023; 37: 3946320231219348.
[20] Engelman JA, Zejnullahu K, Mitsudomi T, Song Y, Hyland C, Park JO, Lindeman N, Gale CM, Zhao X, Christensen J, Kosaka T, Holmes AJ, Rogers AM, Cappuzzo F, Mok T, Lee C, Johnson BE, Cantley LC and Jänne PA. MET amplification leads to gefitinib resistance in lung cancer by activating ERBB3 signaling. Science 2007; 316: 1039-1043.
[21] Hwang SY, Wi K, Yoon G, Lee CJ, Lee SI, Jung JG, Jeong HW, Kim JS, Choi CH, Na CS, Shim JH and Lee MH. Licochalcone D inhibits skin epidermal cells transformation through the regulation of AKT signaling pathways. Biomol Ther (Seoul) 2023; 31: 682-691.
[22] Otto T and Sicinski P. Cell cycle proteins as promising targets in cancer therapy. Nat Rev Cancer 2017; 17: 93-115.
[23] Malumbres M and Barbacid M. Cell cycle, CDKs and cancer: a changing paradigm. Nat Rev Cancer 2009; 9: 153-166.
[24] Xie Q, He Z, Tan L, Li M, Zhuang M, Liu C, Chen S, Jin L and Sui Y. Hesperetin induces apoptosis in lung squamous carcinoma cells via G2/M cycle arrest, inhibition of the Notch1 pathway and activation of endoplasmic reticulum stress. Int J Mol Med 2025; 55: 77.
[25] Marchi S, Giorgi C, Suski JM, Agnoletto C, Bononi A, Bonora M, De Marchi E, Missiroli S, Patergnani S, Poletti F, Rimessi A, Duszynski J, Wieckowski MR and Pinton P. Mitochondria-ros crosstalk in the control of cell death and aging. J Signal Transduct 2012; 2012: 329635.
[26] Dixon SJ, Lemberg KM, Lamprecht MR, Skouta R, Zaitsev EM, Gleason CE, Patel DN, Bauer AJ, Cantley AM, Yang WS, Morrison B 3rd and Stockwell BR. Ferroptosis: an iron-dependent form of nonapoptotic cell death. Cell 2012; 149: 1060-1072.
[27] Doll S, Proneth B, Tyurina YY, Panzilius E, Kobayashi S, Ingold I, Irmler M, Beckers J, Aichler M, Walch A, Prokisch H, Trumbach D, Mao G, Qu F, Bayir H, Fullekrug J, Scheel CH, Wurst W, Schick JA, Kagan VE, Angeli JP and Conrad M. ACSL4 dictates ferroptosis sensitivity by shaping cellular lipid composition. Nat Chem Biol 2017; 13: 91-98.
[28] Feng L, Zhao K, Sun L, Yin X, Zhang J, Liu C and Li B. SLC7A11 regulated by NRF2 modulates esophageal squamous cell carcinoma radiosensitivity by inhibiting ferroptosis. J Transl Med 2021; 19: 367.

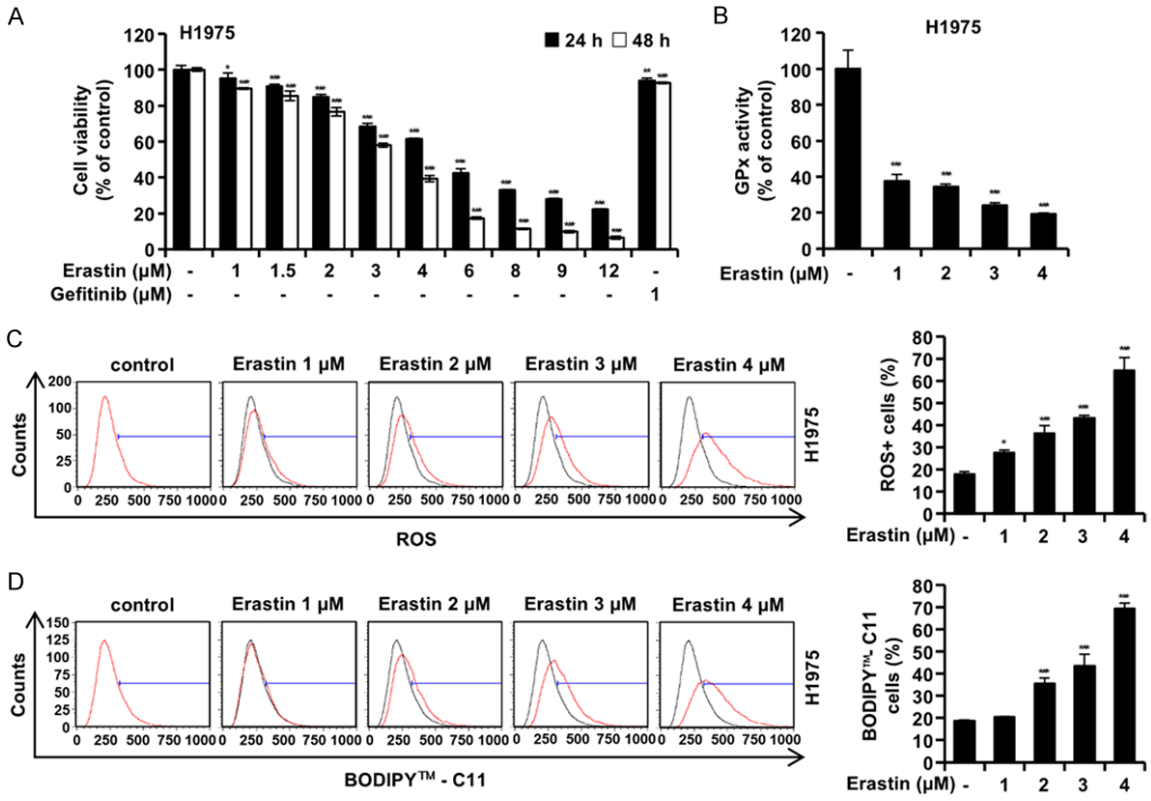

Supplementary Figure 1. Erastin-induced ferroptotic cell death in NCI-H1975 cells. The cells were treated with erastin (1-12 μM) or gefitinib (1 μM) for 24 or 48 h. A. Cell viability using MTT assay. B-D. Cells were treated with erastin (1, 2, 3, and 4 uM) for 48 h. B. GPx activity. C. Intracellular ROS level accessed by flow cytometry using Cell-ROX Green. D. Lipid ROS level measured by BODIPY-C11. Results are shown as mean ± standard deviation (n=3). *P<0.05 and ***P<0.001 compared to the control group (*p* values were obtained via Tukey's post hoc test).